Stress Analysis of Parachutes Using Finite Elements

WILLIAM M. MULLINS* AND DONALD T. REYNOLDS†
Northrop Corporation, Newbury Park, Calif.

An analytical method has been developed for determining the unique shape and internal load distribution that satisfies equilibrium and boundary conditions for a parachute under the influence of known riser and aerodynamic forces. The parachute is treated as a deformable membrane, using finite elements with nonlinear elastic properties to represent the structure. An iterative procedure, performed by a digital computer, is used to find the equilibrium shape. The method is applicable to polysymmetric parachutes which have meridional members (cords or radial tapes) that can be assumed to carry all meridional forces in the canopy. Reefed and nonreefed configurations can be analyzed, and the canopy may be fully or partially inflated. Predicted canopy shapes and failure loads are shown to agree with aerial drop test results.

Nomenclature

a = angle between suspension line and canopy axis (convergence angle) deg
k_p = differential pressure curve integration factor
L = length, in.
M = number of gores
N = unit load, lb/in.
N_R = component of N_ψ normal to meridian, lb/in.
P = load, lb
p = differential pressure, lb/in.^{2}
p' = differential pressure coefficient
R = radius of curvature, in.
r = local projected radius of canopy, in.
S = length of horizontal member, in.
V = axial load at confluence of suspension lines, lb
α = projection of gore half angle in plane normal to meridian, radian
Δ = incremental change
ΔS = length of model meridional segment, in.
ϵ = unit strain, in./in.
ϕ = angle between line perpendicular to meridian and canopy axis, radian
ψ = lobe included half angle, radian

Subscripts

H = horizontal member
M = manufactured
o = skirt
R = meridional member (radial tape)
s = suspension line
θ = circumferential direction
ϕ = meridional direction
ψ = direction of horizontal member

Introduction

THE stresses in a parachute canopy are dependent on the inflated shape, which in turn depends on the stress distribution. This interaction requires that the solutions of stresses and shape be obtained simultaneously. It is understandable, therefore, that much of the effort in parachute stress analysis is concerned with canopy shapes.

The earliest analytical studies of parachute shapes and stresses were performed at the Royal Aircraft Establishment between 1919 and 1923 by a number of investigators including G. I. Taylor and R. A. Jones.[3] The theoretical canopy shape (known as the Taylor zero-hoop stress shape) that was derived has served as the basis for most theoretical work until recent times. Taylor formulated the equations of equilibrium and continuity in a lobed gore, and showed that his equation in general form is equivalent to the general membrane equation.

In 1942, Stevens and Johns[4] considered the case of a parachute with a finite number of suspension lines extending over the canopy. The cords were made shorter than the gore panels so that the cloth carried only hoop stress.

Jager[5] developed a method in 1952 for estimating the maximum horizontal ribbon and radial tape stresses in conical ribbon parachutes. The upper portion of the canopy was assumed to be a cone with zero meridional stress and the lower portion was assumed to be an ellipsoid, with zero hoop tension. Further effort was directed by Topping[6] in 1955 toward fitting functional curves to observed canopy shapes. Modifications of the Taylor shape resulted in improved correlation with the canopy profiles observed in photographs of parachutes in steady descent. Heinrich[7] developed a method for computing canopy cloth stresses for a known profile and pressure distribution. This is the method given in the parachute Handbook.[8] In 1968, Ross[9] set up and solved a set of differential equations to determine the shape and stress distribution in a flat, circular parachute in steady descent.

Roberts[10-11] developed a theoretical aeroelastic model for an inflating parachute and obtained a numerical solution for the shape and stress distribution of a flat circular parachute with uniform pressure distribution. In the stress analysis of an early version of the Apollo main parachute, Ranes[12] used a method which accounted for the relationship between the membrane stresses and the meridional radius of curvature. The pressure distribution data obtained by Melzig[13] in wind-tunnel tests of inflating parachutes was utilized, and the radial tape profile was assumed to be elliptical. Strain compatibility, based on laboratory load-strain data, was used to select a best-fit ellipse.

During the development of the latest Apollo Earth Landing System,[14] a computational algorithm was evolved which gives a rational method for determining the stress distribution in a parachute canopy. This method, which is the subject of the present paper, determines the unique shape and stress distribution that satisfies equilibrium and boundary conditions for a given parachute and applied loading. The method was further extended by use of the Apollo test data in a one year

Presented as Paper 70-1195 at the AIAA Aerodynamic Deceleration Systems Conference, Dayton, Ohio, September 14–16, 1970; received October 16, 1970; revision received July 22, 1971. This work was supported by NASA contract NAS 9-8131.[1-2]

Index categories: Aircraft Deceleration Systems; Post-Entry Deceleration Systems and Flight Mechanics.

* Engineer Specialist, Recovery Systems Group, Ventura Division. Member AIAA.

† Senior Engineer, Research Group, Ventura Division.

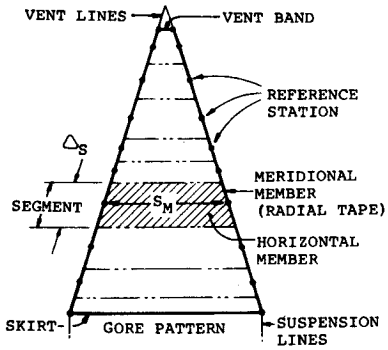

Fig. 1 Structural model of gore.

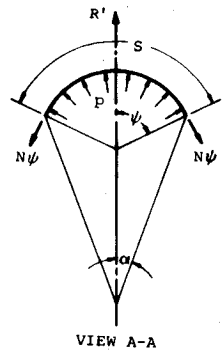

Fig. 3 Lobe geometry and loads.

study program sponsored by NASA Manned Spacecraft Center.[2]

Theory

As a parachute inflates, it deforms to a shape that results in force equilibrium in all members. The summation of the aerodynamic forces acting on the canopy is reacted by the riser force, and the aerodynamic force on each canopy member is reacted by forces from adjacent members. At any time during the inflation process the parachute may be treated as a static problem by use of D'Alembert's principle, as is customary in structural analysis. The first step in the structural analysis of a parachute is to determine the equilibrium shape and stress distribution for the condition and state of inflation being investigated. The analysis derived here provides a method for achieving this end.

Much effort has been directed toward predicting riser forces (for example, Ref. 1) and this is the easiest quantity to measure in tests. Much less is known about the aerodynamic forces acting on the parachute canopy. The approach taken in this analysis is to specify the riser load and adjust the magnitude of the aerodynamic forces, in accordance with a specified pressure distribution curve, to give equilibrium. Only the component normal to the surface of the canopy material is considered, with skin friction being neglected. It is the same for the D'Alembert forces; only the normal component is considered, so that these two forces can be combined algebraically. The net resultant is used instead of differential pressure for dynamic conditions.

The parachute is represented by a structural model made up of simple members capable of carrying uniaxial tension only. Each gore of the canopy is divided into a number of segments, conveniently spaced along the meridians, from the skirt to the vent as shown in Fig. 1.

Each segment is defined by its length along the meridional member, the length of the horizontal member connecting adjacent meridional members, and the load strain curves for these members as determined from laboratory tests. Loads and geometry are computed at reference stations located on the meridional members at the midpoints of the segments.

The following simplifying assumptions are made. 1) All meridional forces are in the meridional members. 2) Meridional curvature is constant over each segment and the curvatures of adjacent segments of the meridian are tangent at their junctions. 3) Horizontal members have no meridional curvature, but each has a constant radius of curvature which is normal to the meridional member at the reference station. 4) Differential pressure acts normal to the surface of the horizontal member only. With these assumptions, each horizontal member may be treated as a free body to determine its end reactions. The computed end reaction is resolved into three mutually perpendicular forces, tangent and normal to the meridional member, from which the loading and radius of curvature of that segment of the meridional member can be computed.

The variation of differential pressure along the meridional member is represented by a nondimensional distribution curve. A solution is obtained for a trial skirt diameter and pressure by establishing equilibrium geometry, first at the skirt then at each successive station to the vent. This trial solution is then examined for compatibility with boundary conditions at the vent. This process is repeated with corrected trial skirt diameters and pressures until the boundary conditions at the vent are satisfied and an over-all force balance is achieved.

A solution begins by establishing equilibrium of the suspension lines and canopy skirt for the trial skirt radius. The equilibrium geometry for an unreefed parachute is shown in Fig. 2. The suspension line convergence angle and the sus-

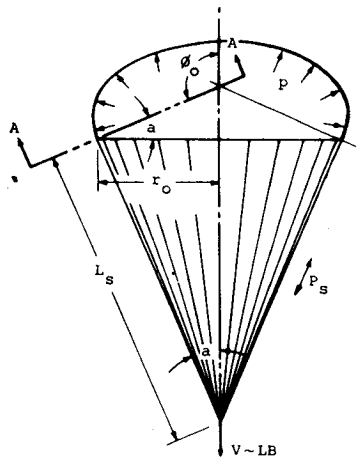

Fig. 2 Parachute profile geometry.

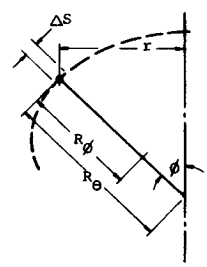

Fig. 4 Loads and geometry along radial.

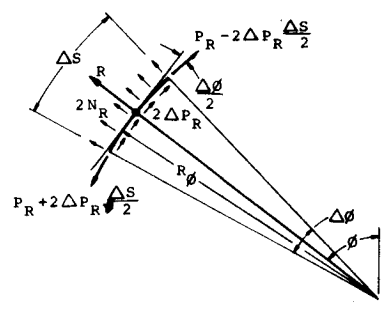

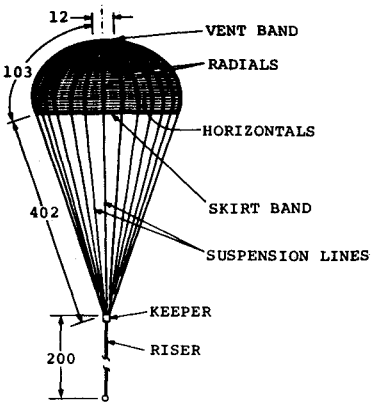

Fig. 5 Drogue chute assembly.

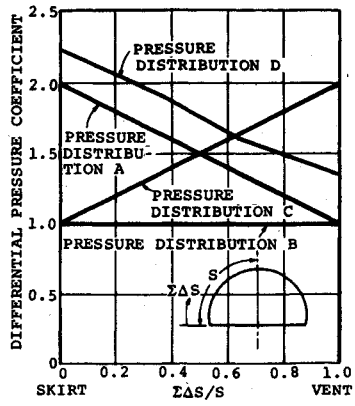

Fig. 7 Arbitrary drogue chute pressure distribution.

pension line loads are given by

$$a = \sin^{-1}[r_0/L_s(1 + \epsilon_s)] \quad (1)$$

$$P_s = V/M \cos a \quad (2)$$

The local differential pressure is expressed by

$$p = p'/k_p \quad (3)$$

where p' is the pressure coefficient from a pressure distribution curve and k_p is an integration factor.

Force equilibrium of the skirt is established by considering the forces and geometry of the segment shown in Fig. 3. From a summation of forces in direction R'

$$N_\psi = (pr \sin\pi/M)/\sin\psi \quad (4)$$

The arc length S is given by

$$S = (2\psi r \sin\pi/M)/\sin\psi \quad (5)$$

The arc length can also be expressed in terms of the manufactured length of the horizontal member and the unit strain

$$S' = S_M(1 + \epsilon_H) \quad (6)$$

A value for the angle ψ is found by iteration to give $S = S'$. This establishes the equilibrium geometry and stress at the skirt for the assumed skirt radius and pressure.

In order to proceed from the skirt segment to the next horizontal member, the loading and geometry of the connecting meridional member must be established. At the skirt, the axial load in the meridional member is equal to the suspension line load $P_{R(\text{skirt})} = P_s$. Resolution of the edge force N_ψ in a horizontal member, results in three mutually perpendicular forces, 1) ΔP_R tangent to the meridional member

$$\Delta P_R = N_\psi \sin(\pi/M) \cos\phi(\cos\psi + \sin\psi \sin\alpha/\cos\alpha) \quad (7)$$

where $\alpha = \sin^{-1}[\sin(\pi/M) \sin\phi]$

2) N_R normal to the meridional member in a plane which includes the central axis

$$N_R = N_\psi[\sin\psi/\cos\alpha - \sin\alpha(\cos\psi + \sin\psi \sin\alpha/\cos\alpha)] \quad (8)$$

3) N_θ a circumferential force

$$N_\theta = N_\psi \cos\pi/M[\cos\psi + \sin\psi \sin\alpha)/\cos\alpha] \quad (9)$$

The edge forces from the two adjacent horizontal members act on each meridional segment. Equilibrium of the meridional member results in the loading shown in Fig. 4.

It is assumed that $\Delta\phi$ is sufficiently small to make $\Delta P_R \Delta S$ negligible compared to P_R. Summation of forces in direction R results in

$$R_\phi = P_R/2N_R \quad (10)$$

Equation (10) defines the meridional radius of curvature R_ϕ in terms of the meridional member loading. The meridional load at any station j is given by

$$P_{R_j} = P_{R(j-1)} - (2\Delta P_R \Delta S/2)_{(j-1)} - (2\Delta P_R \Delta S/2)_j \quad (11)$$

Length of segment j is determined from its initial length and unit strain under load P_R

$$\Delta S_j = \Delta S_j'(1 + \epsilon_R)_j \quad (12)$$

The change in angle ϕ over segment j is given by

$$\Delta\phi_j = \Delta S_j/R_{\phi j} \quad (13)$$

Since it is assumed that the meridional radius of curvature $R_{\phi j}$ is constant over a segment and that the arcs of adjacent segments are tangent at their junction, the geometry of the meridional member is established.

A value of R_ϕ that gives equilibrium for the second segment is established by iteration of Eqs. (3–13). This procedure is repeated for each segment, in turn, from skirt to vent. At the vent, over-all axial force balance and boundary conditions are checked and if necessary the skirt radius, r_0, and the pressure integration factor k_p are revised for a new trial solution. This process is continued until axial force balance and boundary conditions are satisfied. A reefed parachute is analyzed in a similar manner except that reefing line forces are included in establishing equilibrium geometry at the skirt.

This analysis has been programmed for solution by digital computer in a Fortran program called CANO. A complete solution for a typical parachute and loading condition requires less than two minutes of execution time on an IBM 360/65 computer. Input consists of parachute constructed geometry, riser load, pressure distribution curve, and material load-strain curves in tabular form. Output includes complete geometric definition of the inflated canopy and load and strain values for each element.

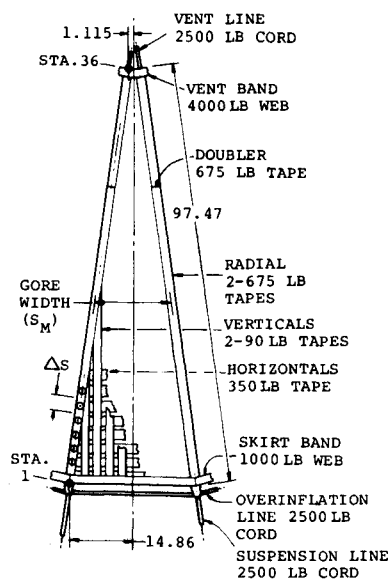

Fig. 6 Drogue chute structural model.

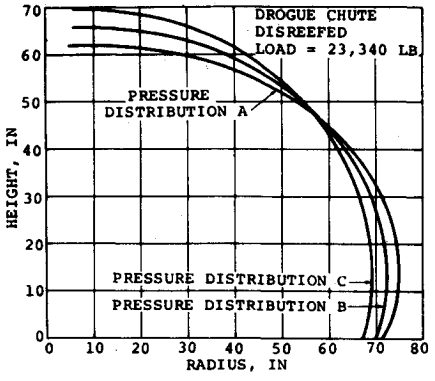

Fig. 8 Drogue canopy profile for various pressure distributions.

Results

Validity of the method has been demonstrated by an extensive comparison of the analytical results with the aerial drop test data obtained in the Apollo Earth Landing System development and qualification programs.

The types of data available include: 1) motion picture coverage from onboard the test vehicle, from chase aircraft, and from test range ground cameras; 2) load-time traces measured at the parachute riser; and 3) failure analyses of drop tests in which parachutes were damaged or destroyed.

Two methods were used to check the analytical results. First, drop test photographs were compared with analytically predicted shapes for the test loading conditions. Since a unique shape is predicted for a given pressure distribution, riser load, and parachute construction, correlation of the predicted and actual canopy shapes is evidence that the internal load and pressure distribution are correct. The second method used to corroborate the analysis is comparison of predicted ultimate strength and failure modes with the results of tests in which failures occurred.

Shape Analysis of the Apollo Drogue Parachute

A comparison of the analytically predicted canopy shape with drop test photographs of the Apollo drogue parachute is presented as the first step in verification of the analysis method.

Structural model

Structural details of the Apollo drogue parachute, a conical ribbon parachute, and the corresponding structural model are given in Figs. 5 and 6. Each model segment includes one horizontal ribbon. Computer input for each segment includes the horizontal ribbon length, a load-strain curve for the ribbon material, meridional length of the segment, and a load-strain curve for the meridional member. Additional model input for the parachute includes suspension line, overinflation line, and vent line lengths and load-strain curves. Canopy pressure distribution is entered in tabular form as a function of location along the meridional member.

Pressure distribution

In order to show the sensitivity of internal loads to pressure distribution, solutions are presented for the three arbitrary distributions shown in Fig. 7. In distribution A, pressure varies linearly from a value of 2 units at the skirt to 1 at the vent. In distribution C this variation is reversed, with peak pressure at the vent. Distribution B is uniform pressure throughout the canopy. Figure 8 shows the variations in canopy profile for the three pressure distributions. Peak pressure at the skirt gives the largest canopy diameter, while peak pressure at the vent gives the largest profile height.

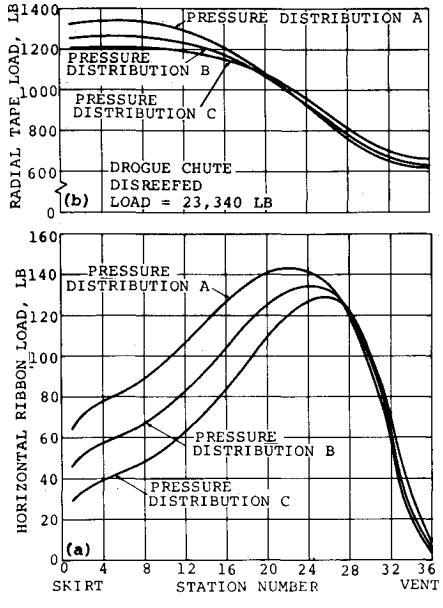

Fig. 9 Horizontal and radial tape loads in drogue chute for various pressure distributions.

The variation in horizontal ribbon loading is shown in Fig. 9a. It is seen that distribution A (peak pressure at the skirt) gives ribbon loads 11% higher than distribution C (peak pressure at the vent). In Fig. 9b radial tape loadings for the three pressure distributions are shown. Distribution A produces the highest loading at the skirt, while distribution C gives higher loads in the crown. This study suggests that profile photographs or strain measurements might be used to infer pressure distribution. Curve D of Fig. 7 is based on data obtained by Melzig[13] in wind-tunnel tests of inflating ribbon parachutes. This distribution is used in the shape analysis that follows.

Shape comparison

Of the three types of photographic coverages available from Apollo drop tests—onboard, air-to-air, and ground-to-air—only the onboard film was adequate to allow shape measurements. Since height data is not obtainable from these plan-view photographs, shape comparisons are based on diameters only, as shown in the plot of Fig. 10. The comparison is intended to show only that the analysis correctly predicts the shape of the canopy since accuracy of the photographic analysis is not sufficient to determine the elongation and resulting stress in the horizontal ribbons. In the lower portion of the canopy, a significant difference exists between predicted and measured diameters. This discrepancy might be attributed to the overinflation line which causes a large canopy development angle (25 deg) at the skirt. This would tend to reduce the pressure differential in the vicinity of the skirt.

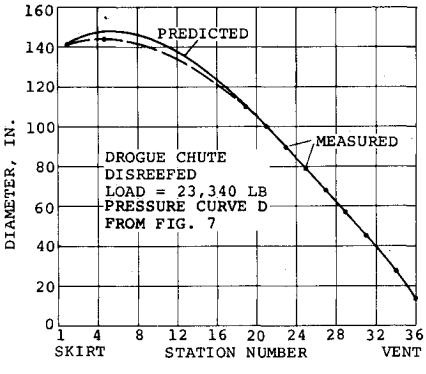

Fig. 10 Comparison of measured and predicted canopy diameters for the drogue chute.

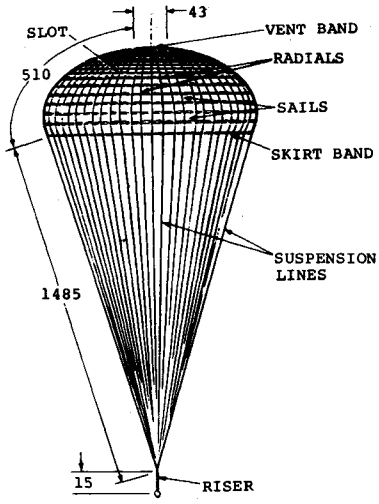

Fig. 11 Main parachute assembly.

Stress Analysis of the Apollo Main Parachute

Structural model

The following discussion is concerned with three versions of the Apollo main parachute that were tested during the development of the Apollo Landing System. Figure 11 shows the complete assembly of the 83.5 ft ringsail parachute and Fig. 12 shows construction details of two typical gores. Such features as sail leading-edge fullness and reinforcing bands are represented in the model by horizontal elements with appropriate geometry and stiffness. The width over which a heavy reinforcing band acts must be estimated, but sensitivity studies show that this is important only locally, since the over-all solution is not sensitive to this modeling. The three versions being considered differ significantly only in the number and strength of reinforcing bands on the sails, as indicated by the coding in Fig. 12. Version 507 is the baseline for this comparison. Version 513 has additional reinforcing tapes added to sails 4–9, and version 519 has additional reinforcements at the trailing edges of sails 5, 9, and 10. Solutions obtained for the three versions under identical external loading give an insight into the effect of the reinforcing bands on the internal load distribution. This difference in construction would, of course, also affect the aerodynamic loading on the

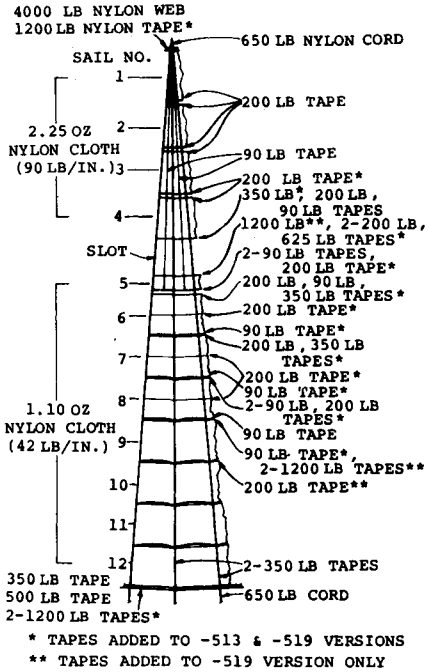

Fig. 12 Structural details of the main parachute canopy.

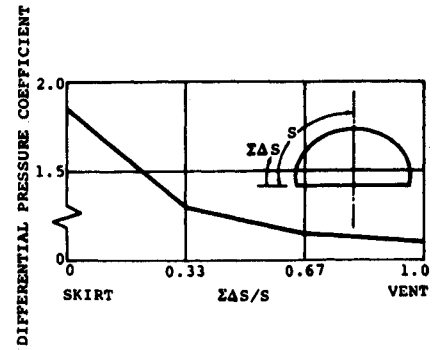

Fig. 13 Fully inflated main parachute pressure distribution.

parachute, but knowledge of the pressure distributions on parachute canopies is not sufficient to evaluate this effect. Slots are accounted for in the solution by traversing the slot segment with no change in meridional member load or slope. Here again, local aerodynamic effects must be neglected since only the gross effect of the porosity provided by the slots can be accounted for aerodynamically. For this analysis, the pressure distribution shown in Fig. 13 for a fully inflated parachute is used. This distribution is based on the data taken from Ref. 13.

Internal load distribution

Separate internal load distributions were computed for each of the three canopy versions, with a riser load of 32,800 lb. A comparison of sail loadings for this condition is shown in Fig. 14. These plots show the variation of the ratio of hoop stress to rated strength. This figure shows the peaking of stresses at the trailing edges of the lower sails, which have fullness in the leading edges. The effects of the heavy reinforcing bands also can be seen. In addition to providing additional strength locally, the bands reduce the stress in adjacent unreinforced areas by reducing the over-all diameter of the canopy. The trailing edges of sails 7–10 are the critically loaded horizontal members. Sail 8 has a load-to-strength ratio of 0.55. The additional reinforcing tapes of the 513 version reduce this ratio to 0.45. In the 513 version the trailing edge of sail 9 is critical, with a load-to-strength ratio of 0.51. Addition of two 1200 lb tapes in the 519 version reduced this ratio to 0.24. The critical area of this canopy is the trailing edge of sail 8, but the load-to-strength ratio is further reduced by the reinforcement of sail 9.

Failure analysis

The prediction of load capability given in Fig. 14 is borne out by failure analyses of parachutes that were damaged in aerial drop tests. Results of the drop tests in which the Apollo main parachutes were subjected to ultimate load tests

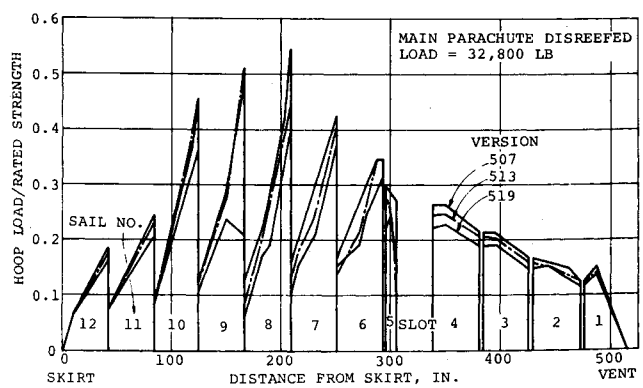

Fig. 14 Sail load—strength ratio for main parachute.

Table 1. Main parachute failure analysis

Parachute version	Measured load	Test damage	Predicted ultimate load	Predicted failure mode
Group 1				
−501	27,660	Gore split beginning at Sail 7 radial seam	31,100	Gore split at Sail 8 radial seam
−501	35,050	Gore split beginning at Sail 8 centerline	31,100	Gore split at Sail 8 radial seam
Group 2				
−509	32,350	No major damage	33,400	Gore split at Sail 9 radial seam
−509	35,060	Gore split beginning at Sail 7 radial seam	33,400	Gore split at Sail 9 radial seam
Group 3				
−515	32,840	No major damage	33,700	Suspension line failure
−515	34,350	Suspension line failure	33,700	Suspension line failure
−519	32,200	Suspension line failure	33,700	Suspension line failure

are given in Table 1. The grouping in this table corresponds in essential structural details to the three structural models discussed previously. The predicted ultimate loads are determined by the stress ratios given in Fig. 14, together with appropriate joint efficiencies and design factors.

References

[1] Mickey, F. E., McEwan, A. J., Ewing, E. G., Huyler, W. C., Jr., and Khajeh-Nouri, B., "Investigation of Prediction Methods for the Loads and Stresses of Apollo Type Spacecraft Parachutes, Volume I—Loads," NVR-6431, June 1970, Northrop Corp., Ventura Div., Newbury Park, Calif.

[2] Mullins, W. M., Reynolds, D. T., Lindh, K. G., and Bottorff, M. R., "Investigation of Prediction Methods for the Loads and Stresses of Apollo Type Spacecraft Parachutes, Volume II–Stresses," NVR-6432, June 1970, Northrop Corp., Ventura Div., Newbury Park, Calif.

[3] Jones, R. A., "On the Aerodynamic Characteristics of Parachutes," R&M 862, June 1923, Aeronautical Research Council, London, England.

[4] Stevens, G. W. H. and Johns, T. F., "The Theory of Parachutes with Cords over the Canopy," R&M 2320, July 1942, Aeronautical Research Council, England.

[5] Jaeger, J. A., Culver, I. H., and Dellavedowa, R. P., "A Study of the Load Distribution in a Conical Ribbon Type Parachute," Report 8641, Aug. 1952, Lockheed Aircraft Corp., Burbank, Calif.

[6] Topping, A. D., Marketos, J. D., and Costakos, N. C., "A Study of Canopy Shapes and Stresses for Parachutes in Steady Descent," TR-55-294 (AD 103 963), Oct. 1955, Wright Air Development Center, Ohio.

[7] Heinrich, H. G. and Jamison, L. R., "Parachute Stress Analysis During Inflation and at Steady State," *Journal of Aircraft*, Vol. 3, No. 1, Jan.-Feb. 1966, pp. 52–58.

[8] "Performance of and Design Criteria for Deployable Aerodynamic Decelerators," ASD-TR-61-579, Dec. 1963, AFFDL, Wright-Patterson Air Force Base, Ohio.

[9] Ross, E. W., Jr., "Approximate Analysis of a Flat, Circular Parachute in Steady Descent," TR-69-51-OSD, Dec. 1968, U.S. Army Natick Lab., Natick, Mass.

[10] Roberts, B. W., "A Contribution to Parachute Inflation Dynamics," 2nd AIAA Aerodynamic Deceleration Conference, Sept. 23–25, 1968, El Centro, Calif.

[11] Roberts, B. W., "The Shape and Stresses in an Arbitrarily Shaped Gore Parachute Under Arbitrary Pressure Distribution," AIAA Paper 70-1197, Sept. 1970, Dayton, Ohio.

[12] Ranes, R., Topp, G., and Utzman, C., "Strength Analysis—Apollo Earth Landing System, Block II," NVR-4055, March 1967, Northrop Corp., Ventura Div., Newbury Park, Calif.

[13] Melzig, H. D. and Saliaris, C., "Pressure Distribution During Parachute Opening," AFFDL-TR-68-135, Feb. 1969, Wright-Patterson Air Force Base, Ohio.

[14] Utzman, C., Mullins, W., Reynolds, D., Farnsworth, R., and Labbe, J., "Strength Analysis—Apollo Block II Earth Landing System, Weight Accommodation Program," NVR-6112A, Sept. 1968, Northrop Corp., Ventura Div., Newbury Park, Calif.